Letter

Engineering anomalous Floquet Majorana modes and their time evolution in a helical Shiba chain

Debashish Mondal [1,2,*] Arnob Kumar Ghosh [1,2,†] Tanay Nag [3,4,‡] and Arijit Saha [1,2,§]
[1] *Institute of Physics, Sachivalaya Marg, Bhubaneswar 751005, India*
[2] *Homi Bhabha National Institute, Training School Complex, Anushakti Nagar, Mumbai 400094, India*
[3] *Department of Physics and Astronomy, Uppsala University, Box 516, 75120 Uppsala, Sweden*
[4] *Department of Physics, BITS Pilani–Hyderabad Campus, Telangana 500078, India*

(Received 12 April 2023; revised 4 July 2023; accepted 20 July 2023; published 4 August 2023)

We theoretically explore the Floquet generation of Majorana end modes (MEMs; both regular 0 modes and anomalous π modes) implementing a periodic sinusoidal modulation in the chemical potential in an experimentally feasible setup based on a one-dimensional chain of magnetic impurity atoms having spin spiral configuration (out-of-plane Néel type) fabricated on the surface of a common bulk s-wave superconductor. We obtain a rich phase diagram in the parameter space, highlighting the possibility of generating multiple 0- and π-MEMs localized at the end of the chain. We also study the real-time evolution of these emergent MEMs, especially when they start to appear in the time domain. These MEMs are topologically characterized by employing the dynamical winding number. We observe that the existing perturbative analysis is unable to explain the numerical findings, indicating the complex mechanism behind the formation of the Floquet Shiba minigap, which is characteristically distinct from other setups, e.g., the Rashba nanowire model. We also discuss the possible experimental parameters in connection to our model. Our work paves the way to realize Floquet MEMs in a magnet-superconductor heterostructure.

DOI: 10.1103/PhysRevB.108.L081403

Introduction. Majorana zero modes (MZMs) associated with topological superconductors (TSCs) [1–7] have been attracting massive attention due to their non-Abelian braiding property, which is proposed to be the elementary building block for fault-tolerant topological quantum computation [8–12]. The idea of MZMs was first proposed by Kitaev through the model of a one-dimensional (1D) spinless p-wave superconductor [1,2]. However, this model is not experimentally feasible due to the unavailability of a 1D p-wave superconductor in nature. Nevertheless, there exists an alternate realistic proposal to engineer 1D Kitaev-like physics in 1D semiconducting nanowire (NW) with strong spin-orbit coupling (SOC), placed in close proximity to a bulk s-wave superconductor in the presence of a Zeeman field [4,5,7,13–16]. A Majorana zero-bias peak, observed in several transport experiments based on hybrid superconductor-semiconductor NW setups, has been interpreted as the indirect signature of the MZMs [15–20].

In recent times, the hunt for MZMs has taken an alternative route based on the helical spin chain [21–33] or magnetic adatoms fabricated on the surface of a bulk s-wave superconductor [34–41]. Physically, the scattering between magnetic impurities and the quasiparticles in the superconductor fosters the formation of Yu-Shiba-Rusinov (YSR) states [42–46] inside the superconducting gap. These YSR states can hybridize among themselves and form YSR or Shiba bands. The helical spin texture and strength of the magnetic impurities play the combined role of SOC and magnetic field, respectively [26,33]. A few experimental proposals based on scanning tunneling microscopy (STM) measurements have also been reported to realize the MZMs associated with the minigap of YSR bands [47–55].

On the other hand, Floquet generation is a sophisticated and versatile way to engineer on-demand topological phases out of a nontopological system [56–75]. The absorption and emission of photons from the driving field lead to the formation of Floquet quasienergy sidebands. These overlapping sidebands trigger the band-gap opening and band inversion resulting in the appearance of Floquet topological modes. The dynamical setup also facilitates the generation of the anomalous topological boundary modes at finite energy, namely, π modes, having no static counterpart. In this exciting direction of Floquet band engineering, the emergence of Floquet Majorana end modes (MEMs) has been explored in 1D p-wave Kitaev chains [67–69], 1D cold-atomic-NW–s-wave-superconductor heterostructures [70,72–74], and also, very recently, in a realistic 1D Rashba NW model [76]. The braiding of these Floquet boundary modes further adds merit to these systems due to their applicability in quantum computations [77–80]. Notwithstanding this, the Floquet generation of MEMs in a realistic helical spin chain model along with their topological characterization is yet to be explored. At this stage, we would like to pursue the answers to the following intriguing questions: (a) Is it possible to generate and topologically characterize Floquet MEMs employing a realistic model based on a helical-Shiba-chain–s-wave-superconductor

*debashish.m@iopb.res.in
†arnob@iopb.res.in
‡tanay.nag@physics.uu.se
§arijit@iopb.res.in

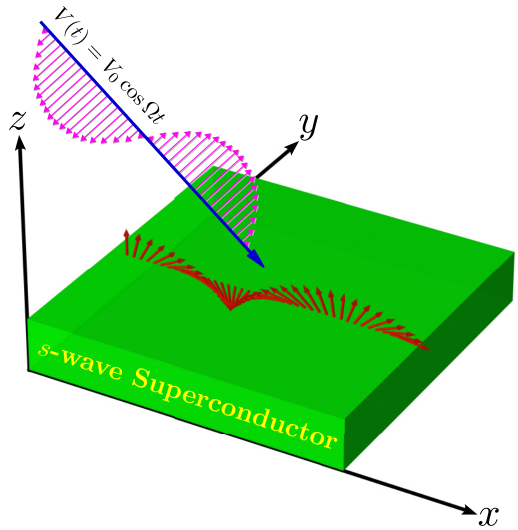

FIG. 1. Schematic representation of our setup. A 1D chain of magnetic adatoms with their spins (red arrows) confined in the xz plane (out-of-plane Néel-type spin spiral configuration) is placed on top of a bulk s-wave superconductor (green).

(magnet-superconductor) heterostructure while starting from a trivial phase? (b) How do these dynamical MEMs within the emergent quasienergy Shiba band evolve with time?

In this Research Letter, we first briefly discuss the underlying static model based on a helical 1D magnetic spin chain proximitized with a common bulk s-wave superconductor [21] (see Fig. 1). We explore the generation of Floquet MEMs (both 0 modes and anomalous π modes) employing an external periodic sinusoidal drive in this setup (see Fig. 2). Afterward, we demonstrate the real-time evolution of the Floquet MEMs (see Fig. 3). We compute the dynamical winding number utilizing the periodized evolution operator to characterize the topological nature of the Floquet MEMs as shown in Fig. 4. We find that the numerically obtained quasienergy spectrum cannot be described by the analytical perturbative analysis where the superconducting part is only renormalized without affecting the normal part in the Bogoliubov–de Gennes (BdG) Hamiltonian (see Fig. 5). We also provide some probable experimental parameters concerning our system of interest.

Static model. We consider the model of a helical spin chain, based on a 1D chain of magnetic impurity atoms mimicking an out-of-plane Néel-type spin spiral (SS) configuration [46] that is fabricated on the surface of a bulk s-wave superconductor [21] (see Fig. 1 for a schematic). We employ the following BdG basis: $\Psi_j = \{c_{j\uparrow}, c_{j\downarrow}, c^\dagger_{j\downarrow}, -c^\dagger_{j\uparrow}\}^{\mathbf{t}}$, where $c^\dagger_{j\uparrow}$ ($c_{j\uparrow}$) and $c^\dagger_{j\downarrow}$ ($c_{j\downarrow}$) represent the quasiparticle creation (annihilation) operators for the spin-up and spin-down sectors, respectively, at lattice site j and $\mathbf{t}$ indicates the transpose operation. Exploiting the BdG basis, we can write an effective 1D Hamiltonian in real space for our system as

$$H = \sum_j \Psi^\dagger_j[-\mu\Gamma_1 + B\cos(j\theta)\Gamma_2 + B\sin(j\theta)\Gamma_3 + \Delta\Gamma_4]\Psi_j + \sum_j \Psi^\dagger_{j,\eta} t_h \Gamma_1 \Psi_{j+1} + \text{H.c.}, \tag{1}$$

where μ, B, θ, Δ, and t_h represent the chemical potential, the magnetic impurity strength, the angle between two adjacent spins, the superconducting pairing gap, and the hopping amplitude, respectively. Also, $\Gamma_1 = \tau_z\sigma_0$, $\Gamma_2 = \tau_0\sigma_z$, $\Gamma_3 = \tau_0\sigma_x$, and $\Gamma_4 = \tau_x\sigma_0$, while the Pauli matrices $\boldsymbol{\tau}$ and $\boldsymbol{\sigma}$ act on the particle-hole and spin ($\uparrow$, $\downarrow$) subspaces, respectively. Here, we assume that all the impurity spins as classical such that they are well separated from each other and do not interact among themselves. The Hamiltonian H [Eq. (1)] preserves chiral symmetry $S = \mathbb{I}_N \otimes \tau_y\sigma_y$, $S^{-1}HS = -H$, and particle-hole symmetry (PHS) $\mathcal{C} = \mathbb{I}_N \otimes \tau_y\sigma_y\mathcal{K}$, $\mathcal{C}^{-1}H\mathcal{C} = -H$, with N and $\mathcal{K}$ representing the number of impurity atoms and the complex-conjugation operation, respectively. However, H breaks the time-reversal symmetry (TRS) $\mathcal{T} = \mathbb{I}_N \otimes i\tau_0\sigma_y\mathcal{K}$: $\mathcal{T}^{-1}H\mathcal{T} \neq H$.

Floquet generation of MEMs. We employ a periodic sinusoidal drive in the on-site chemical potential to generate the Floquet TSC phase hosting MEMs. We choose the initial static Hamiltonian [Eq. (1)] such that it resides in the trivial

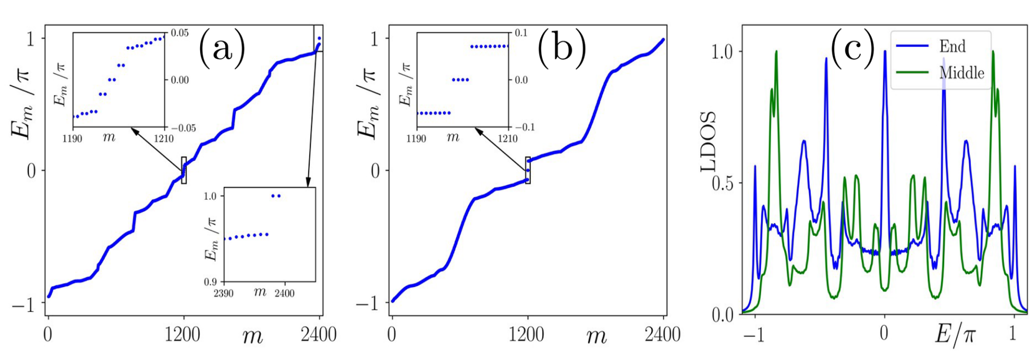

FIG. 2. (a) and (b) The quasienergy spectra of the Floquet operator for $B/\Delta = 2$ and $B/\Delta = 3$, respectively. Floquet 0- and π-MEMs are highlighted in the top-left and bottom-right insets, respectively. (c) The energy-resolved normalized LDOS computed at the end (blue curve) and middle (green curve) of the chain for $B/\Delta = 2$. The green peaks represent the emergent Shiba modes within the Floquet quasienergy spectrum. Here, we consider a 1D chain of 600 lattice sites, and we choose the model parameters $(\mu/\Delta, t_h/\Delta, \theta) = (4, 1, 2\pi/3)$, $\Omega/\Delta = 1.5$, and $V_0/\Delta = 5$.

phase to begin with. The driving protocol reads

$$V(t) = \sum_j \Psi_j^\dagger [V_0 \cos(\Omega t)\Gamma_1]\Psi_j, \tag{2}$$

where V_0 and Ω $(= 2\pi/T)$ represent the strength and frequency of the drive, respectively, while T stands for the time period of the external drive. The periodicity of the drive $V(t+T) = V(t)$ is ensured in the full time-dependent Hamiltonian $H(t) = H + V(t)$ as $H(t+T) = H(t)$. We work in the real-time-domain picture, and the time-evolution operator in terms of the time-ordered (TO) product reads as [81]

$$U(t,0) = \mathrm{TO}\exp\left[-\int_0^t dt' H(t')\right] = \prod_{j=0}^{M-1} U(t_j + \delta t, t_j), \tag{3}$$

where $U(t_j + \delta t, t_j) = e^{-iH(t_j)\delta t}$, with $\delta t = t/M$, $t_j = j\delta t$, and M being the total number of Trotterization steps. The Floquet operator $U(T,0)$ is the time-evolution operator computed at $t = T$. Here, $U(T,0)$ serves the purpose of the dynamical analog of the Hamiltonian. Thus we diagonalize $U(T,0)$ to procure the quasienergy spectrum for our system. The corresponding quasienergy $E_m \in [-\pi, \pi]$. We demonstrate the quasienergy spectrum as a function of the state index m in Figs. 2(a) and 2(b) for different impurity strengths ($B/\Delta = 2$ and $B/\Delta = 3$, respectively, which indicate the nontopological regime in the static model; see Supplemental Material (SM) [82]). For $B/\Delta = 2$, we obtain two MEMs (one mode per end) at both quasienergy $E = 0$ and quasienergy $E = \pi$ [see the top-left and bottom-right insets, respectively, in Fig. 2(a)]. For $B/\Delta = 3$, we highlight the generation of multiple MEMs at $E = 0$ [see the inset in Fig. 2(b)]. The generation of MEMs at quasienergy π is unique to the Floquet systems only and does not have any static analog, and this also serves as the prime result of this Research Letter considering the Shiba chain model. Apart from 0 energy, MEMs may also appear at finite energy ($\pm\pi$) in Floquet systems due to the presence of PHS in the underlying BdG Hamiltonian. Thus the states having quasienergy 0 and $\pi \equiv -\pi$ can be their own antiparticle [70]. In Fig. 2(c), we depict the energy-resolved local density of states (LDOS) computed at the end (blue curve) and middle (green curve) of the chain. Note that the LDOS is normalized by its maximum value throughout this Research Letter. The peaks at $E = 0, \pm\pi$, denoted by the blue curve, indicate the presence of Floquet MEMs when the LDOS is computed at the end of the chain. On the other hand, the green curve in Fig. 2(c) does not exhibit any peak at $E = 0$ or $\pm\pi$; peaks in this curve indicate an emergent bulk Floquet quasienergy Shiba band within the superconducting gap as the LDOS is calculated at the middle of the chain. Thus the 0 and $\pm\pi$ modes are truly boundary modes without having any weightage at the bulk. Moreover, the separation between the lowest green peaks (close to 0 and $\pm\pi$) indicates the corresponding dynamical topological gap.

Time evolution of the Floquet MEMs. The real-time dependence of the driving protocol motivates us to pursue the time evolution of the emergent Floquet MEMs [81]. To this end, we diagonalize $U(t,0)$ and illustrate the instantaneous eigenvalue spectra $E(t)$ as a function of time t in Fig. 3(a). At $t = 0$, the system is a trivial superconductor. Afterwards, we observe that both the 0- and π-MEMs continue to appear and disappear in the Floquet TSC phase as a function of time t before one reaches the full time period T; this can be identified distinctly from Fig. 3(a). To unveil the footprints of the MEMs at different time instances, we consider four time slices: time point 1 at $t = 0.28T$ with only 0 modes, time point 2 at $t = 0.63T$ with only π modes, time point 3 at $t = 0.9T$ with both 0 and π modes, and time point 4 at $t = T$ when both 0 and π modes present. The LDOSs associated with 0 and/or

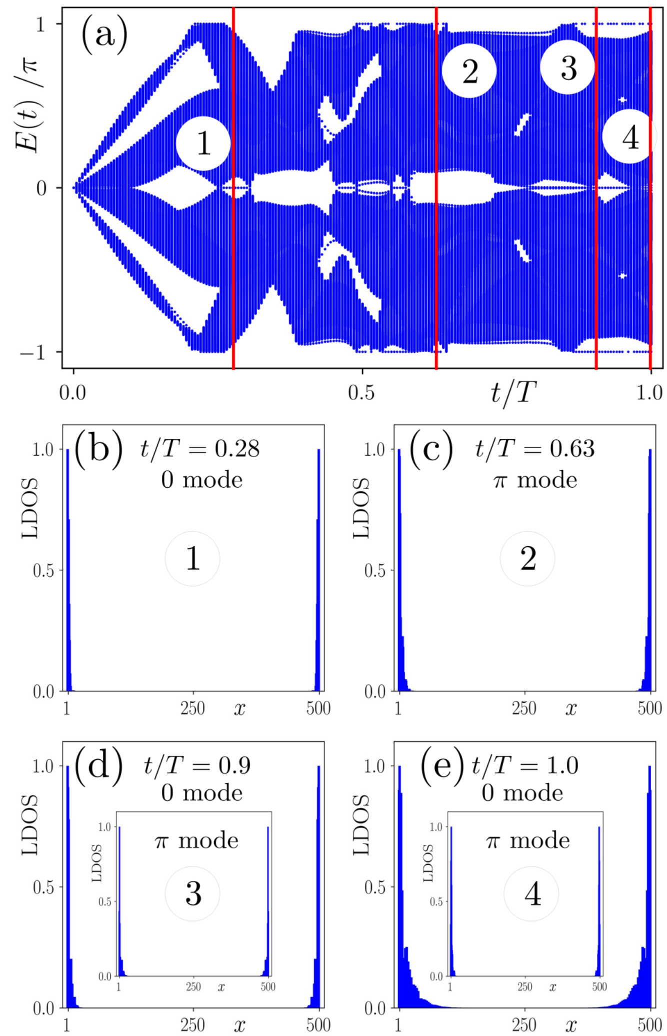

FIG. 3. (a) The time-dependent eigenvalue spectra of the time-evolution operator $U(t,0)$ as a function of time t. Both the 0 and π modes appear and disappear with time during the time interval $t \in [0, T]$. We consider four time points: $t = 0.28T$ with only 0 modes (time point 1), $t = 0.63T$ with only π modes (time point 2), $t = 0.9T$ with both 0 and π modes (time point 3), and $t = T$ with both 0 and π modes (time point 4). (b), (c), (d) and (e) denote the time-dependent site resolved LDOSs for 0 and/or π modes corresponding to time points 1, 2, 3 and 4, respectively. Clearly, at $t/T = 0.28$ ($t/T = 0.63$) only 0 modes (π modes) are present, while at $t/T = 0.9$ and $t/T = 1$ both the 0- and π-MEMs appear. Here, we consider a 1D chain of 500 lattice sites, and all the model parameters take the values as in Fig. 2.

π modes corresponding to time points 1–4 are demonstrated with respect to the length of the chain in Figs. 3(b)–3(e), respectively. It is worth mentioning here that both the 0 modes and the π modes are sharply localized at the two ends of the 1D chain.

Topological characterization of the dynamical MEMs. The broken translational symmetry in H [Eq. (1)] rules out the computation of the topological invariant in momentum space. However, one can employ twisted boundary conditions (TBCs) in a real-space geometry to topologically characterize the system [76]. To this end, we connect the two ends of the 1D chain and embed a hypothetical flux η through it. The flux induces a Peierls phase substitution to the hopping amplitude as $t_h \to t_h e^{i\eta j}$ with $j \in \mathbb{Z}$ [76]. The Hamiltonian H [Eq. (1)] and the time-evolution operator $U(t,0)$ [Eq. (3)] become an explicit function of η such that $H \to H(\eta)$ and $U(t,0) \to U(\eta;t,0)$. We enforce periodic boundary conditions (PBCs) employing the constraint on η as $N\eta = 2\pi$. Here, we note that depending on the angle between two successive impurity spins θ, the PBCs can be achieved only for a few specific values of N (see SM [82] for details). To characterize the MEMs with a distinct topological invariant, we also need to invoke the periodized evolution operator, constructed employing TBCs, defined as [65,82,93,94]

$$U_\epsilon(\eta;t,0) = U(\eta;t,0)[U(\eta;T,0)]_\epsilon^{-t/T}. \tag{4}$$

Here, ϵ stands for the 0 and π gap. Afterward, we exploit the chiral symmetry operator to define a dynamical winding number W_ϵ to topologically characterize the MEMs appearing at quasienergy ϵ [76,82], as

$$W_\epsilon = \left| \frac{i}{2\pi} \int_{-\pi}^{\pi} d\eta \, \mathrm{Tr}\big[\{U_\epsilon^{\pm}(\eta;T/2,0)\}^{-1} \partial_\eta U_\epsilon^{\pm}(\eta;T/2,0)\big] \right|. \tag{5}$$

One can obtain $U_0^{\pm}(\eta;T/2,0)$ [$U_\pi^{\pm}(\eta;T/2,0)$] by writing the periodized evolution operator employing the chiral basis (see SM [82] for details). Here, W_ϵ counts the number of Floquet MEMs in the TSC phase residing at a particular quasienergy ϵ.

We depict the dynamical winding numbers W_0 and W_π in the $V_0 - \Omega$ plane in Figs. 4(a) and 4(b), respectively, while the color bar represents the number of Floquet MEMs. In certain parameter spaces, one can notice that the number of 0 and/or π modes becomes more than 1. For better clarity, we also illustrate W_0 and W_π as a function of Ω for three different fixed values of V_0 in Figs. 4(c), and 4(d), respectively. Thus the appearance of multiple Floquet MEMs is also supported by the outcome of the dynamical winding number. We further show the bulk gap at quasienergies 0 (G_0) and π (G_π) in the $V_0 - \Omega$ plane in Figs. 4(e) and 4(f), respectively. Each gap closing in G_0 and G_π corresponds to a jump in W_0 and W_π, respectively, indicating a topological phase transition. This one-to-one mapping between the dynamical winding number W_ϵ and the bulk gap G_ϵ is evident from Fig. 4.

Perturbative analysis. Having investigated the problem numerically, we employ two perturbative schemes, namely, the Floquet perturbation theory (FPT) [81,95–97] and the Brillouin-Wigner (BW) perturbation theory [98,99], to examine the high-amplitude driving $V_0 \gg t_h$ and the high-frequency driving $\Omega \gg t_h$, respectively. We find that the

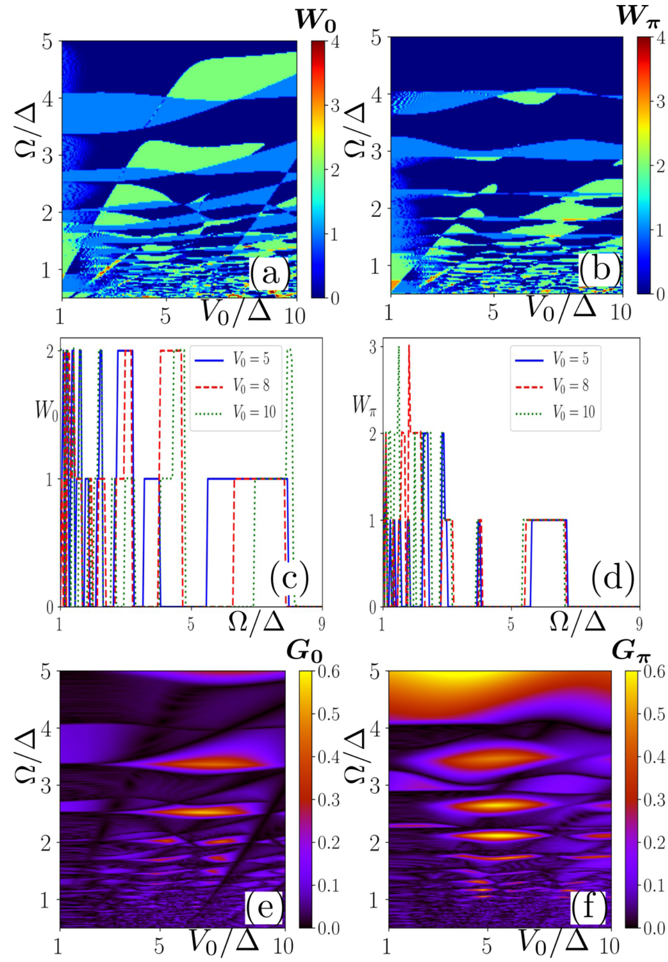

FIG. 4. (a) and (b) The dynamical winding numbers W_0 and W_π, respectively, in the $V_0 - \Omega$ plane. Here, W_ϵ characterizes the Floquet MEMs residing at the quasienergy gap ϵ. (c) and (d) W_0 and W_π, respectively, as a function of Ω for three fixed values, $V_0/\Delta = 5$ (solid blue curve), 8 (dashed red curve), and 10 (dotted green curve), for better clarity. (e) and (f) The quasienergy gap around quasienergies 0 and π, respectively. We choose $B/\Delta = 5$ (topological regime of the static model), and the rest of the model parameters take the same values as in Fig. 2.

superconducting term is renormalized in the leading order as $\Delta_{\mathrm{FPT}}^{\mathrm{eff}} = \Delta\, J_0(\frac{2V_0}{\Omega})$ and $\Delta_{\mathrm{BW}}^{\mathrm{eff}} = \Delta\,(1 - \frac{V_0^2}{2\Omega^2})$ for the FPT and BW techniques, respectively, where $J_0(x)$ is the 0th Bessel function of the first kind (see SM [82] for details). Notably, the normal part of the BdG Hamiltonian remains unaffected by such perturbations in the leading order.

We compute the quasienergy spectrum in the real space for the effective Floquet Hamiltonian. In Fig. 5, we compare the quasienergy spectra obtained from the FPT Hamiltonian (blue dots), the BW Hamiltonian (red dots), and the exact Floquet operator (green dots). We demonstrate the cases where FPT and BW perturbation theory can successfully predict the zero-energy modes for very few choices of parameters. However, FPT and BW perturbation theory fail to anticipate the zero-energy mode and the overall quasienergy profile for most of the parameter space, even though the above theories are applicable to those parameter choices. In Fig. 5(a), we

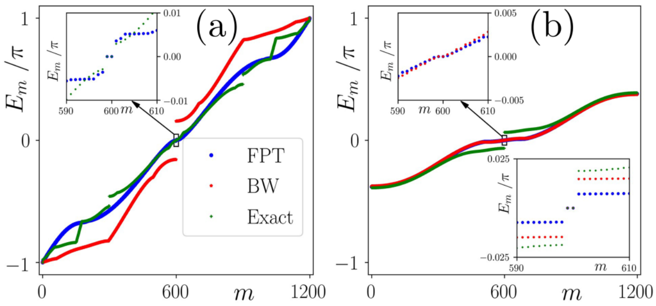

FIG. 5. Comparison of the eigenvalue spectra E_m as a function of m, obtained from the FPT (blue dots), the BW perturbation theory (red dots), and the exact Floquet operator (green dots). In (a), we depict the eigenvalue spectra for $(V_0/\Delta, \Omega/\Delta) = (10, 3)$, while in the inset we show the modes near quasienergy zero. We choose $(V_0/\Delta, \Omega/\Delta) = (5, 10)$ for (b), while the zoomed-in spectra near zero quasienergy are shown in the top-left inset. In the bottom-right inset, we demonstrate the eigenvalue spectra for $(V_0/\Delta, \Omega/\Delta) = (5, 6.5)$. We choose a 1D chain of 300 lattice sites, and the rest of the model parameters are the same as in Fig. 2.

depict an instant where FPT matches with the exact numerics to a certain extent; interestingly, the zero-energy modes are successfully predicted. However, the BW perturbation theory severely fails to mimic the exact spectrum [see the inset in Fig. 5(a) for better clarity]. On the other hand, in Fig. 5(b), FPT and BW perturbation theory exhibit similar spectra, while the exact numerics is drastically different as FPT and BW perturbation theory exhibit (exact numerics exhibits) a gapless (gapped) feature around zero quasienergy [see the top-left inset in Fig. 5(b) for better clarity]. However, as we lower the drive amplitude and increase the drive frequency, FBT and BW perturbation theory can sometimes mimic the zero energy modes as noticed from the exact numerics [see the bottom-right inset in Fig. 5(b)]. The match between theory and numerics is not rigorous, but only accidental. Hence neither the FPT nor the BW perturbation theory can satisfactorily explain the emergence of MEMs in the driven system.

The numerical findings apprehend that the drive and magnetic impurity both simultaneously modify normal and superconducting parts of the BdG Hamiltonian. Since the above perturbation theories do not modify the normal part of the BdG Hamiltonian, indicating that FPT and BW perturbation theory cannot capture the modulation of the Shiba minigap in the presence of the time-periodic drive. Note that the emergent Floquet Shiba minigap comprises both the renormalized superconducting part and the normal part. More precisely, the closed-form expression of the dynamical Shiba gap is not tractable as the driving term, namely, the chemical potential, is hidden inside the static Shiba bands in a complex manner. Finding an appropriate theory to understand the Floquet Shiba minigap in a driven helical spin chain is far more complex than anticipated and beyond the scope of this Research Letter. Interestingly, our numerical investigation with the quasienergy spectrum indicates that the driven chain starts hosting Floquet MEMs for substantially lower strengths of magnetic impurity compared with the static case [82].

Plausible experimental realization. Having demonstrated the generation of Floquet MEMs theoretically, here we discuss a possible way to realize our setup experimentally. The most suitable superconducting candidate material may be bulk Nb (110) since it has the highest possible superconducting gap of $\Delta = 1.51$ meV among the conventional superconductors [51]. Afterward, one may fabricate magnetic adatoms such as Mn or Cr over the bulk Nb (110) employing STM-based single-atom manipulation methods [49,50,54,100]. This method could provide better tunability of the angle between two impurity spins. Following our model, we consider the scenario described in Fig. 2(a), and to this end, the other model parameters can take the values $t_h = \Delta = 1.51$ meV, $B = 2\Delta = 3.02$ meV, and $\mu = 4\Delta = 6.04$ meV. Moreover, the periodic sinusoidal modulation of the on-site chemical potential can be achieved through an ac gate voltage having an amplitude $V_0 = 5\Delta = 7.55$ meV and frequency $\Omega \approx 3.44$ THz for the generation of Floquet 0- and π-MEMs.

Summary and conclusion. To summarize, in this Research Letter, we demonstrate an experimentally feasible way to engineer Floquet MEMs employing a helical spin chain model (in the form of a Néel-type SS configuration fabricated on the surface of an s-wave superconductor) and periodic modulation of the chemical potential. We obtain a rich phase diagram in the parameter space, allowing us to realize both Floquet 0-MEMs and Floquet π-MEMs in the emergent quasienergy band. We also investigate the time evolution and tunability of the number of Floquet MEMs. The 0- and π-MEMs are always sharply localized at the two ends of the system. We topologically characterize the MEMs utilizing the dynamical winding number in a real-space picture. Our study indicates the limitation of perturbative calculations that only refer to the renormalization of the superconducting part in the BdG Hamiltonian in mimicking the exact numerical result. Therefore our work reveals an angle where magnetic impurity physics gets intertwined with the Floquet drive to render the p-wave superconducting gap, which is extremely nontrivial to anticipate *a priori*. This complex phenomenon can be easily distinguished from the Floquet Rashba NW physics, where the normal part of the BdG Hamiltonian is only modified [76]. Our numerical findings clearly show a substantial reduction in the strength of the magnetic impurity to host the Floquet MEMs compared with that for the static case [82]. However, we leave a detailed microscopic understanding of the emergent dynamical Shiba minigap (0 and π gaps) for future studies. We also provide probable experimental parameters to realize our setup. These Floquet MEMs are relatively robust as we start from the trivial phase and possibly can be probed by the STM signal.

Acknowledgments. D.M., A.K.G., and A.S. acknowledge SAMKHYA–High-Performance Computing Facility provided by the Institute of Physics, Bhubaneswar, for numerical computations. D.M. and A.K.G. thank P. Chatterjee for stimulating discussions.

[1] A. Y. Kitaev, Unpaired Majorana fermions in quantum wires, Phys.-Usp. **44**, 131 (2001).
[2] A. Kitaev, Periodic table for topological insulators and superconductors, in *Advances in Theoretical Physics: Landau Memorial Conference*, AIP Conf. Proc. No. 1134 (American Institute of Physics, Melville, NY, 2009), pp. 22–30.
[3] X.-L. Qi and S.-C. Zhang, Topological insulators and superconductors, Rev. Mod. Phys. **83**, 1057 (2011).
[4] M. Leijnse and K. Flensberg, Introduction to topological superconductivity and Majorana fermions, Semicond. Sci. Technol. **27**, 124003 (2012).
[5] J. Alicea, New directions in the pursuit of Majorana fermions in solid state systems, Rep. Prog. Phys. **75**, 076501 (2012).
[6] C. Beenakker, Search for Majorana fermions in superconductors, Annu. Rev. Condens. Matter Phys. **4**, 113 (2013).
[7] R. Aguado, Majorana quasiparticles in condensed matter, Riv. Nuovo Cimento **40**, 523 (2017).
[8] D. A. Ivanov, Non-Abelian Statistics of Half-Quantum Vortices in p-Wave Superconductors, Phys. Rev. Lett. **86**, 268 (2001).
[9] M. Freedman, A. Kitaev, M. Larsen, and Z. Wang, Topological quantum computation, Bull. Am. Math. Soc. **40**, 31 (2003).
[10] A. Kitaev, Fault-tolerant quantum computation by anyons, Ann. Phys. (Amsterdam) **303**, 2 (2003).
[11] A. Stern, Non-Abelian states of matter, Nature (London) **464**, 187 (2010).
[12] C. Nayak, S. H. Simon, A. Stern, M. Freedman, and S. Das Sarma, Non-Abelian anyons and topological quantum computation, Rev. Mod. Phys. **80**, 1083 (2008).
[13] Y. Oreg, G. Refael, and F. von Oppen, Helical Liquids and Majorana Bound States in Quantum Wires, Phys. Rev. Lett. **105**, 177002 (2010).
[14] R. M. Lutchyn, J. D. Sau, and S. Das Sarma, Majorana Fermions and a Topological Phase Transition in Semiconductor-Superconductor Heterostructures, Phys. Rev. Lett. **105**, 077001 (2010).
[15] V. Mourik, K. Zuo, S. M. Frolov, S. R. Plissard, E. P. A. M. Bakkers, and L. P. Kouwenhoven, Signatures of Majorana fermions in hybrid superconductor-semiconductor nanowire devices, Science **336**, 1003 (2012).
[16] A. Das, Y. Ronen, Y. Most, Y. Oreg, M. Heiblum, and H. Shtrikman, Zero-bias peaks and splitting in an Al–InAs nanowire topological superconductor as a signature of Majorana fermions, Nat. Phys. **8**, 887 (2012).
[17] L. P. Rokhinson, X. Liu, and J. K. Furdyna, The fractional a.c. Josephson effect in a semiconductor–superconductor nanowire as a signature of Majorana particles, Nat. Phys. **8**, 795 (2012).
[18] A. D. K. Finck, D. J. Van Harlingen, P. K. Mohseni, K. Jung, and X. Li, Anomalous Modulation of a Zero-Bias Peak in a Hybrid Nanowire-Superconductor Device, Phys. Rev. Lett. **110**, 126406 (2013).
[19] S. M. Albrecht, A. P. Higginbotham, M. Madsen, F. Kuemmeth, T. S. Jespersen, J. Nygård, P. Krogstrup, and C. M. Marcus, Exponential protection of zero modes in Majorana islands, Nature (London) **531**, 206 (2016).
[20] M. T. Deng, S. Vaitiekėnas, E. B. Hansen, J. Danon, M. Leijnse, K. Flensberg, J. Nygård, P. Krogstrup, and C. M. Marcus, Majorana bound state in a coupled quantum-dot hybrid-nanowire system, Science **354**, 1557 (2016).
[21] S. Nadj-Perge, I. K. Drozdov, B. A. Bernevig, and A. Yazdani, Proposal for realizing Majorana fermions in chains of magnetic atoms on a superconductor, Phys. Rev. B **88**, 020407(R) (2013).
[22] F. Pientka, L. I. Glazman, and F. von Oppen, Topological superconducting phase in helical Shiba chains, Phys. Rev. B **88**, 155420 (2013).
[23] J. Klinovaja, P. Stano, A. Yazdani, and D. Loss, Topological Superconductivity and Majorana Fermions in RKKY Systems, Phys. Rev. Lett. **111**, 186805 (2013).
[24] F. Pientka, L. I. Glazman, and F. von Oppen, Unconventional topological phase transitions in helical Shiba chains, Phys. Rev. B **89**, 180505(R) (2014).
[25] K. Pöyhönen, A. Westström, J. Röntynen, and T. Ojanen, Majorana states in helical Shiba chains and ladders, Phys. Rev. B **89**, 115109 (2014).
[26] N. Sedlmayr, J. M. Aguiar-Hualde, and C. Bena, Flat Majorana bands in two-dimensional lattices with inhomogeneous magnetic fields: Topology and stability, Phys. Rev. B **91**, 115415 (2015).
[27] S. Hoffman, J. Klinovaja, and D. Loss, Topological phases of inhomogeneous superconductivity, Phys. Rev. B **93**, 165418 (2016).
[28] M. H. Christensen, M. Schecter, K. Flensberg, B. M. Andersen, and J. Paaske, Spiral magnetic order and topological superconductivity in a chain of magnetic adatoms on a two-dimensional superconductor, Phys. Rev. B **94**, 144509 (2016).
[29] G. M. Andolina and P. Simon, Topological properties of chains of magnetic impurities on a superconducting substrate: Interplay between the Shiba band and ferromagnetic wire limits, Phys. Rev. B **96**, 235411 (2017).
[30] D. Sticlet and C. Morari, Topological superconductivity from magnetic impurities on monolayer $NbSe_2$, Phys. Rev. B **100**, 075420 (2019).
[31] S. Rex, I. V. Gornyi, and A. D. Mirlin, Majorana modes in emergent-wire phases of helical and cycloidal magnet-superconductor hybrids, Phys. Rev. B **102**, 224501 (2020).
[32] N. Mohanta, S. Okamoto, and E. Dagotto, Skyrmion control of Majorana states in planar Josephson junctions, Commun. Phys. **4**, 163 (2021).
[33] R. Hess, H. F. Legg, D. Loss, and J. Klinovaja, Prevalence of trivial zero-energy subgap states in nonuniform helical spin chains on the surface of superconductors, Phys. Rev. B **106**, 104503 (2022).
[34] J. D. Sau and E. Demler, Bound states at impurities as a probe of topological superconductivity in nanowires, Phys. Rev. B **88**, 205402 (2013).
[35] S. Nakosai, Y. Tanaka, and N. Nagaosa, Two-dimensional p-wave superconducting states with magnetic moments on a conventional s-wave superconductor, Phys. Rev. B **88**, 180503(R) (2013).
[36] H.-Y. Hui, P. M. R. Brydon, J. D. Sau, S. Tewari, and S. D. Sarma, Majorana fermions in ferromagnetic chains on the surface of bulk spin-orbit coupled s-wave superconductors, Sci. Rep. **5**, 8880 (2015).
[37] J. Röntynen and T. Ojanen, Topological Superconductivity and High Chern Numbers in 2D Ferromagnetic Shiba Lattices, Phys. Rev. Lett. **114**, 236803 (2015).

[38] G. Sharma and S. Tewari, Yu-Shiba-Rusinov states and topological superconductivity in Ising paired superconductors, Phys. Rev. B **94**, 094515 (2016).

[39] A. Theiler, K. Björnson, and A. M. Black-Schaffer, Majorana bound state localization and energy oscillations for magnetic impurity chains on conventional superconductors, Phys. Rev. B **100**, 214504 (2019).

[40] M. Mashkoori, S. Pradhan, K. Björnson, J. Fransson, and A. M. Black-Schaffer, Identification of topological superconductivity in magnetic impurity systems using bulk spin polarization, Phys. Rev. B **102**, 104501 (2020).

[41] R. L. R. C. Teixeira, D. Kuzmanovski, A. M. Black-Schaffer, and L. G. G. V. D. da Silva, Enhanced Majorana bound states in magnetic chains on superconducting topological insulator edges, Phys. Rev. B **102**, 165312 (2020).

[42] H. Shiba, Classical spins in superconductors, Prog. Theor. Phys. **40**, 435 (1968).

[43] O. Deb, S. Hoffman, D. Loss, and J. Klinovaja, Yu-Shiba-Rusinov states and ordering of magnetic impurities near the boundary of a superconducting nanowire, Phys. Rev. B **103**, 165403 (2021).

[44] F. von Oppen and K. J. Franke, Yu-Shiba-Rusinov states in real metals, Phys. Rev. B **103**, 205424 (2021).

[45] J. Ortuzar, S. Trivini, M. Alvarado, M. Rouco, J. Zaldivar, A. L. Yeyati, J. I. Pascual, and F. S. Bergeret, Yu-Shiba-Rusinov states in two-dimensional superconductors with arbitrary Fermi contours, Phys. Rev. B **105**, 245403 (2022).

[46] P. Chatterjee, S. Pradhan, A. K. Nandy, and A. Saha, Tailoring the phase transition from topological superconductor to trivial superconductor induced by magnetic textures of a spin chain on a p-wave superconductor, Phys. Rev. B **107**, 085423 (2023).

[47] S. Nadj-Perge, I. K. Drozdov, J. Li, H. Chen, S. Jeon, J. Seo, A. H. MacDonald, B. A. Bernevig, and A. Yazdani, Observation of Majorana fermions in ferromagnetic atomic chains on a superconductor, Science **346**, 602 (2014).

[48] A. Yazdani, Visualizing Majorana fermions in a chain of magnetic atoms on a superconductor, Phys. Scr. **2015**, 014012 (2015).

[49] H. Kim, A. Palacio-Morales, T. Posske, L. Rózsa, K. Palotás, L. Szunyogh, M. Thorwart, and R. Wiesendanger, Toward tailoring Majorana bound states in artificially constructed magnetic atom chains on elemental superconductors, Sci. Adv. **4**, eaar5251 (2018).

[50] L. Schneider, S. Brinker, M. Steinbrecher, J. Hermenau, T. Posske, M. dos Santos Dias, S. Lounis, R. Wiesendanger, and J. Wiebe, Controlling in-gap end states by linking nonmagnetic atoms and artificially-constructed spin chains on superconductors, Nat. Commun. **11**, 4707 (2020).

[51] L. Schneider, P. Beck, T. Posske, D. Crawford, E. Mascot, S. Rachel, R. Wiesendanger, and J. Wiebe, Topological Shiba bands in artificial spin chains on superconductors, Nat. Phys. **17**, 943 (2021).

[52] P. Beck, L. Schneider, L. Rózsa, K. Palotás, A. Lászlóffy, L. Szunyogh, J. Wiebe, and R. Wiesendanger, Spin-orbit coupling induced splitting of Yu-Shiba-Rusinov states in antiferromagnetic dimers, Nat. Commun. **12**, 2040 (2021).

[53] D. Wang, J. Wiebe, R. Zhong, G. Gu, and R. Wiesendanger, Spin-Polarized Yu-Shiba-Rusinov States in an Iron-Based Superconductor, Phys. Rev. Lett. **126**, 076802 (2021).

[54] L. Schneider, P. Beck, J. Neuhaus-Steinmetz, L. Rózsa, T. Posske, J. Wiebe, and R. Wiesendanger, Precursors of Majorana modes and their length-dependent energy oscillations probed at both ends of atomic Shiba chains, Nat. Nanotechnol. **17**, 384 (2022).

[55] D. Crawford, E. Mascot, M. Shimizu, P. Beck, J. Wiebe, R. Wiesendanger, H. O. Jeschke, D. K. Morr, and S. Rachel, Majorana modes with side features in magnet-superconductor hybrid systems, npj Quantum Mater. **7**, 117 (2022).

[56] T. Oka and H. Aoki, Photovoltaic Hall effect in graphene, Phys. Rev. B **79**, 081406(R) (2009).

[57] T. Kitagawa, T. Oka, A. Brataas, L. Fu, and E. Demler, Transport properties of nonequilibrium systems under the application of light: Photoinduced quantum Hall insulators without Landau levels, Phys. Rev. B **84**, 235108 (2011).

[58] N. H. Lindner, G. Refael, and V. Galitski, Floquet topological insulator in semiconductor quantum wells, Nat. Phys. **7**, 490 (2011).

[59] M. S. Rudner, N. H. Lindner, E. Berg, and M. Levin, Anomalous Edge States and the Bulk-Edge Correspondence for Periodically Driven Two-Dimensional Systems, Phys. Rev. X **3**, 031005 (2013).

[60] G. Usaj, P. M. Perez-Piskunow, L. E. F. Foa Torres, and C. A. Balseiro, Irradiated graphene as a tunable Floquet topological insulator, Phys. Rev. B **90**, 115423 (2014).

[61] P. M. Perez-Piskunow, G. Usaj, C. A. Balseiro, and L. E. F. F. Torres, Floquet chiral edge states in graphene, Phys. Rev. B **89**, 121401(R) (2014).

[62] A. Eckardt, Colloquium: Atomic quantum gases in periodically driven optical lattices, Rev. Mod. Phys. **89**, 011004 (2017).

[63] S. Yao, Z. Yan, and Z. Wang, Topological invariants of Floquet systems: General formulation, special properties, and Floquet topological defects, Phys. Rev. B **96**, 195303 (2017).

[64] T. Oka and S. Kitamura, Floquet engineering of quantum materials, Annu. Rev. Condens. Matter Phys. **10**, 387 (2019).

[65] M. Rudner and N. Lindner, Band structure engineering and non-equilibrium dynamics in Floquet topological insulators, Nat. Rev. Phys. **2**, 229 (2020).

[66] T. Nag and B. Roy, Anomalous and normal dislocation modes in Floquet topological insulators, Commun. Phys. **4**, 157 (2021).

[67] M. Thakurathi, A. A. Patel, D. Sen, and A. Dutta, Floquet generation of Majorana end modes and topological invariants, Phys. Rev. B **88**, 155133 (2013).

[68] M. Benito, A. Gómez-León, V. M. Bastidas, T. Brandes, and G. Platero, Floquet engineering of long-range p-wave superconductivity, Phys. Rev. B **90**, 205127 (2014).

[69] A. C. Potter, T. Morimoto, and A. Vishwanath, Classification of Interacting Topological Floquet Phases in One Dimension, Phys. Rev. X **6**, 041001 (2016).

[70] L. Jiang, T. Kitagawa, J. Alicea, A. R. Akhmerov, D. Pekker, G. Refael, J. I. Cirac, E. Demler, M. D. Lukin, and P. Zoller, Majorana Fermions in Equilibrium and in Driven Cold-Atom Quantum Wires, Phys. Rev. Lett. **106**, 220402 (2011).

[71] A. A. Reynoso and D. Frustaglia, Unpaired Floquet Majorana fermions without magnetic fields, Phys. Rev. B **87**, 115420 (2013).

[72] D. E. Liu, A. Levchenko, and H. U. Baranger, Floquet Majorana Fermions for Topological Qubits in Superconducting

Devices and Cold-Atom Systems, Phys. Rev. Lett. **111**, 047002 (2013).

[73] M. Thakurathi, D. Loss, and J. Klinovaja, Floquet Majorana fermions and parafermions in driven Rashba nanowires, Phys. Rev. B **95**, 155407 (2017).

[74] Z. Yang, Q. Yang, J. Hu, and D. E. Liu, Dissipative Floquet Majorana Modes in Proximity-Induced Topological Superconductors, Phys. Rev. Lett. **126**, 086801 (2021).

[75] C. Bao, P. Tang, D. Sun, and S. Zhou, Light-induced emergent phenomena in 2D materials and topological materials, Nat. Rev. Phys. **4**, 33 (2022).

[76] D. Mondal, A. K. Ghosh, T. Nag, and A. Saha, Topological characterization and stability of Floquet Majorana modes in Rashba nanowires, Phys. Rev. B **107**, 035427 (2023).

[77] R. W. Bomantara and J. Gong, Simulation of Non-Abelian Braiding in Majorana Time Crystals, Phys. Rev. Lett. **120**, 230405 (2018).

[78] R. W. Bomantara and J. Gong, Quantum computation via Floquet topological edge modes, Phys. Rev. B **98**, 165421 (2018).

[79] B. Bauer, T. Pereg-Barnea, T. Karzig, M.-T. Rieder, G. Refael, E. Berg, and Y. Oreg, Topologically protected braiding in a single wire using Floquet Majorana modes, Phys. Rev. B **100**, 041102(R) (2019).

[80] A. Matthies, J. Park, E. Berg, and A. Rosch, Stability of Floquet Majorana Box Qubits, Phys. Rev. Lett. **128**, 127702 (2022).

[81] A. K. Ghosh, T. Nag, and A. Saha, Time evolution of Majorana corner modes in a Floquet second-order topological superconductor, Phys. Rev. B **107**, 035419 (2023).

[82] See Supplemental Material at http://link.aps.org/supplemental/10.1103/PhysRevB.108.L081403 for details of the topological phase boundaries and static winding number, characterization of the Floquet MEMs via the dynamical winding number, details of FPT and BW results, details of quasi-1D results (static and dynamic cases), and a general discussion, which includes Refs. [83–92].

[83] Q. Niu and D. J. Thouless, Quantised adiabatic charge transport in the presence of substrate disorder and many-body interaction, J. Phys. A **17**, 2453 (1984).

[84] Q. Niu, D. J. Thouless, and Y.-S. Wu, Quantized Hall conductance as a topological invariant, Phys. Rev. B **31**, 3372 (1985).

[85] T. Kitagawa, E. Berg, M. Rudner, and E. Demler, Topological characterization of periodically driven quantum systems, Phys. Rev. B **82**, 235114 (2010).

[86] S. Ryu, A. P. Schnyder, A. Furusaki, A. W. W. Ludwig, Topological insulators and superconductors: tenfold way and dimensional hierarchy, New J. Phys. **12**, 065010 (2010).

[87] T.-P. Choy, J. M. Edge, A. R. Akhmerov, and C. W. J. Beenakker, Majorana fermions emerging from magnetic nanoparticles on a superconductor without spin-orbit coupling, Phys. Rev. B **84**, 195442 (2011).

[88] P. Titum, E. Berg, M. S. Rudner, G. Refael, and N. H. Lindner, Anomalous Floquet-Anderson Insulator as a Nonadiabatic Quantized Charge Pump, Phys. Rev. X **6**, 021013 (2016).

[89] S. Roy and G. J. Sreejith, Disordered Chern insulator with a two-step Floquet drive, Phys. Rev. B **94**, 214203 (2016).

[90] C.-K. Chiu, J. C. Y. Teo, A. P. Schnyder, and S. Ryu, Classification of topological quantum matter with symmetries, Rev. Mod. Phys. **88**, 035005 (2016).

[91] M. Fruchart, Complex classes of periodically driven topological lattice systems, Phys. Rev. B **93**, 115429 (2016).

[92] D. Vu, Dynamic bulk-boundary correspondence for anomalous Floquet topology, Phys. Rev. B **105**, 064304 (2022).

[93] D. Vu, R.-X. Zhang, Z.-C. Yang, and S. D. Sarma, Superconductors with anomalous Floquet higher-order topology, Phys. Rev. B **104**, L140502 (2021).

[94] A. K. Ghosh, T. Nag, and A. Saha, Dynamical construction of quadrupolar and octupolar topological superconductors, Phys. Rev. B **105**, 155406 (2022).

[95] B. Mukherjee, A. Sen, D. Sen, and K. Sengupta, Dynamics of the vacuum state in a periodically driven Rydberg chain, Phys. Rev. B **102**, 075123 (2020).

[96] A. Sen, D. Sen, and K. Sengupta, Analytic approaches to periodically driven closed quantum systems: methods and applications, J. Phys.: Condens. Matter **33**, 443003 (2021).

[97] S. Ghosh, K. Saha, and K. Sengupta, Hinge-mode dynamics of periodically driven higher-order Weyl semimetals, Phys. Rev. B **105**, 224312 (2022).

[98] T. Mikami, S. Kitamura, K. Yasuda, N. Tsuji, T. Oka, and H. Aoki, Brillouin-Wigner theory for high-frequency expansion in periodically driven systems: Application to Floquet topological insulators, Phys. Rev. B **93**, 144307 (2016).

[99] A. K. Ghosh, G. C. Paul, and A. Saha, Higher order topological insulator via periodic driving, Phys. Rev. B **101**, 235403 (2020).

[100] D. M. Eigler and E. K. Schweizer, Positioning single atoms with a scanning tunnelling microscope, Nature (London) **344**, 524 (1990).